Supporting information

Ni-doped Cu oxide catalysts for ORR: suppressing H_2O_2 formation by engineering chemical strain

Sekhar Kumar Biswal and Chinmoy Ranjan*

Department of Inorganic and Physical Chemistry, Indian Institute of Science,

Bangalore560012 (India)

Corresponding author: ranjan@iisc.ac.in

Table of Contents: *Page No.*

I. Details of electrochemical measurements

ORR measurements were carried out in a three-electrode rotating ring disc electrode (RRDE) cell (Pine Instruments) at room temperature with continuous O_2 flow and different rotation speeds (400-2025 rpm). The scan rates for linear sweep voltammetry (LSV) and cyclic voltammetry (CV) measurements were set to 5 and 20 mV/s, respectively. The stability of ORR was assessed for a duration of 10 hours under O_2 flow at 1600 rpm, with measurements taken at 0.7 V. To perform electrochemical impedance spectroscopy (EIS) measurements, a sinusoidal ac perturbation of 10 mV was applied over the frequency range of 0.01-10^5 Hz at a voltage of 0.6 V. The catalysts were tested for accelerated durability by cycling them for 3000 potential cycles from 0.6 V to 1.0 V at a scan rate of 100 mV/s.

The amount of H_2O_2 and electron count were measured with a RRDE during ORR measurements. While the ring potential was set to 1.5 V, the disc swept at a rate of 5 mV/s. The following formula was used to determine the electron number (n) and the percentage of H_2O_2:

$$n = 4 \times \frac{i_d}{i_d + \frac{i_R}{N}} \quad \text{----------(S1)}$$

$$\%\, H_2O_2 = 200 \times \frac{\frac{i_r}{N}}{i_d + \frac{i_r}{N}} \quad \text{----------(S2)}$$

i_d and i_r represent the disc and ring currents, respectively, and N represents the ring's collection efficiency (25%).

II. Preparation of Ni-doped CuO_x electrodes ($Cu[Ni]O_x$/Au)

Similar to the previous report, the Ni-doped CuO_x catalysts ($Cu[Ni]O_x$) were prepared using the electroless deposition method followed by thermal annealing.[1] In a typical procedure, Stoichiometric amounts of $Cu(NO_3)_2.3H_2O$ and $NiSO_4.6H_2O$ were dissolved in 10 ml of deionized water in 2:8, 4:6, 6:4, and 8:2, respectively. The total concentration of metal ions

was kept at 0.06 M. The electrode was made by immersing a polycrystalline, 5 mm diameter, electrochemically cleaned gold disc in the solutions for 5 minutes and thermally treating it for 3 hours at 300℃.

III. Details of characterization Techniques

Scanning electron microscopy (SEM) and Energy dispersive X-ray spectroscopy (EDX) analyses were performed on a Carl Zeiss Ultra 55 FESEM apparatus with a SE2 detector. The accelerating voltage was kept at 15 kV for SEM imaging and 20 kV for SEM-EDX mapping to study samples' surface morphologies and elemental ratios.

Transmission electron microscopy (TEM) images were obtained using a JEOL JEM 2100F electron microscope fitted with an Olympus SIS Keen View G2 CCD camera for data collection. The operational voltage was held steady at 200 kilovolts during the entire process, and the elemental analysis was carried out with the help of the Oxford Instruments INCA EDX system. The samples were prepared by dispersing them in ethanol and then drop-casting them onto a lacey carbon copper TEM grid.

Collecting thin-film X-ray diffraction (XRD) patterns in Grazing Incidence of Diffraction (GID) mode was performed using a Bruker D8 discover X-ray diffractometer equipped with Cu Kα radiation.

X-ray photoelectron spectroscopy (XPS) and Auger electron spectroscopy (AES) were performed on catalytic samples using a Thermo Scientific K-Alpha XPS system with an Al Kα source. A focal point size of 400 micrometers was designated. The scanning step size was configured to be 0.10 electron volts (eV), while the pass energy value was 50.0 eV. All reported binding energies were adjusted by referencing them to the C 1s signal at 284.8 eV.

The Raman spectra were acquired using a Renishaw In-Via Raman Microscope, employing an excitation wavelength of 785 nm at room temperature. The electrochemical Raman spectra

were acquired in a 0.1 M NaOH solution saturated with O_2 using a custom-designed three-electrode Teflon cell. The counter electrode consisted of platinum wire, while the reference electrode was an Ag/AgCl (sat. KCl) electrode. The experimental setup described in a prior publication was employed to conduct in-situ Raman measurements.[1,2] The Raman spectra were acquired using a laser exposure time of 10 seconds and a source power of 3 milliwatts (mW). The ultimate spectrum was computed by taking the average of two data sets. The Raman spectra were obtained from submerged samples using an exposure time of 15 seconds. The spectra averaged over two accumulations, and a source laser power of 30 mW was used. In the in-situ experiments, the potential was incrementally stepped to the predetermined potential value and subsequently maintained for six minutes. The Raman collection commenced after one minute of potential application for each instance. The Raman Spectrometer was calibrated using a Si wafer at 520.5 cm^{-1} before each experiment.

Polycrystalline Au foil was used as a catalyst substrate for the in situ electrochemical Raman spectroscopy experiment. The Au foil was roughened electrochemically using a process established by Liu et al.[3] The method consists of 25 cycles of oxidation-reduction potential scanning between -0.28V (hold time 10s) and 1.22V (hold time 5s) vs. Ag/AgCl in 0.1M NaCl solution at a scan rate of 500 mV/s. The roughened Au was washed with ultrapure water before being electrochemically cleaned with cycling.

IV. Material characterization

The Ni-doped CuO_x catalysts synthesized on Au substrate ($Cu[Ni]O_x$/Au) were characterized using Raman spectroscopy, TEM, SEM, and XRD, as shown in **Figure S1**. **Figure S1(a)** shows an optical picture of $Cu_{0.8}Ni_{0.2}O_x$/Au acquired from a microscope paired with a Raman instrument. The area associated with the green and yellow regions corresponds to the catalyst and Gold (Au) substrate regions, respectively. The $Cu_{0.8}Ni_{0.2}O_x$/Au electrode morphology was

characterized by TEM, as shown in **Figure S1(b)**, revealing a layered structured morphology. **Figure S1(c)** shows a similar morphology discovered in SEM analysis. The SEM and TEM elemental mapping of the $Cu_{0.8}Ni_{0.2}O_x$/Au electrode in the designated region depicted in **Figures S1(d) and S1(e)** indicate that the distribution of Cu and Ni is uniform over the whole area. **Figure S1(f)** shows that the SEM-EDX analysis corroborated the elemental composition of Cu and Ni in the electrodes, revealing that the ratio of metal ions in the electrodes is identical to that of the precursor solution. The X-ray diffraction (XRD) pattern of the $Cu_{0.8}Ni_{0.2}O_x$/Au electrode was obtained using grazing angle incidence mode (GID), as depicted in **Figure S1(g)**. The XRD patterns reveal the existence of $Ni(OH)_2$ and CuO species near the surface; the Au substrate was also visible. **Figure S2-S5** displays the SEM images and EDX spectra of the Cu[Ni]O_x/Au electrodes. **Figure S6** exhibits the SEM-EDX mapping of the elements in all four doped samples, revealing a uniform distribution of copper (Cu) and nickel (Ni).

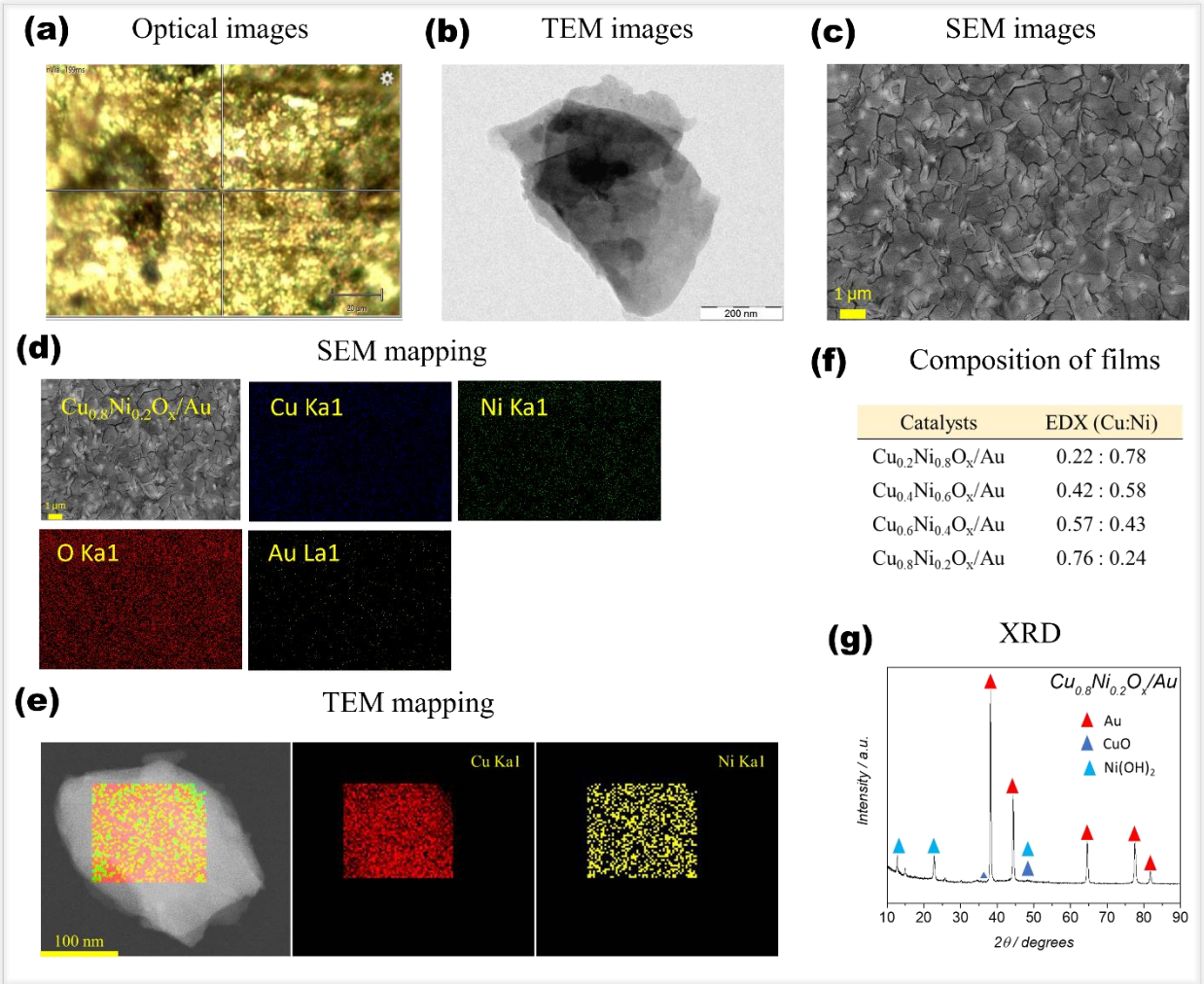

Catalysts	EDX (Cu:Ni)
$Cu_{0.2}Ni_{0.8}O_x/Au$	0.22 : 0.78
$Cu_{0.4}Ni_{0.6}O_x/Au$	0.42 : 0.58
$Cu_{0.6}Ni_{0.4}O_x/Au$	0.57 : 0.43
$Cu_{0.8}Ni_{0.2}O_x/Au$	0.76 : 0.24

Figure S1. *Characterization of the catalyst: (a) optical image, (b) TEM image, (c) SEM image, (d) SEM-EDX elemental mapping, and (e) TEM-EDX elemental mapping show how Ni and Cu are distributed in the catalyst ($Cu_{0.8}Ni_{0.2}O_x/Au$). (f) Metal composition of the as-prepared oxides determined by SEM-EDX. (g) XRD pattern of $Cu_{0.8}Ni_{0.2}O_x/Au$.*

V. Elemental analysis of electrodes

The elemental analysis of the as-prepared electrodes was carried out using Scanning electron microscopy (SEM) in combination with Energy Dispersive X-ray analysis (EDX) (**Figures S2-S5**).

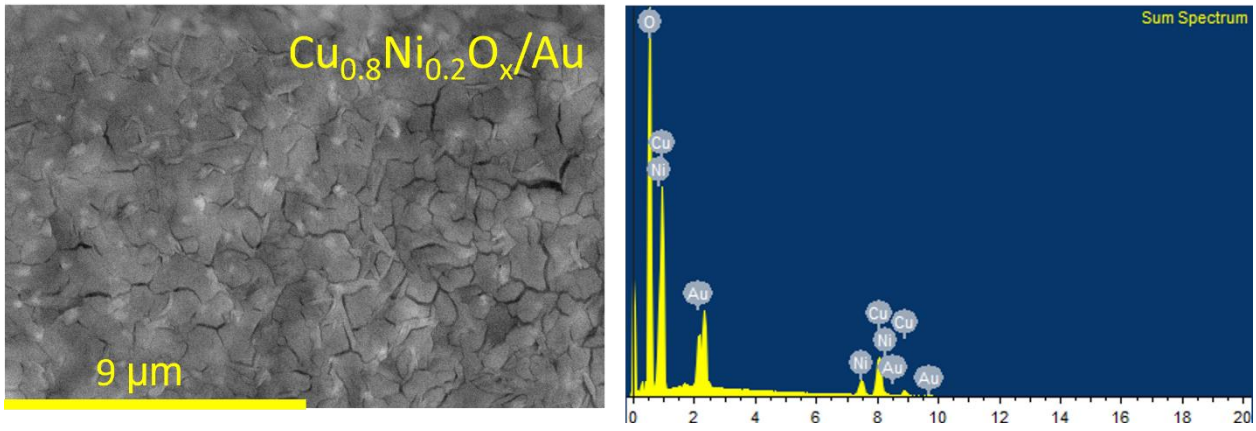

Figure S2. *SEM Image and EDX spectrum for $Cu_{0.8}Ni_{0.2}O_x$/Au as-prepared electrode. EDX revealed a composition of 18.59% Cu, 5.95% Ni, 74.50% O, and 0.95% Au.*

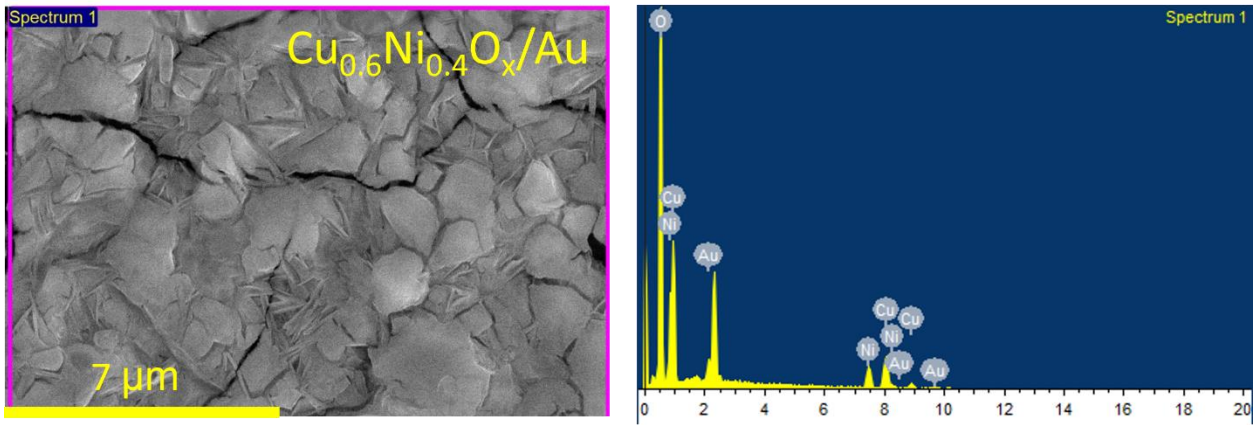

Figure S3. *SEM Image and EDX spectrum for $Cu_{0.6}Ni_{0.4}O_x$/Au as-prepared electrode. EDX revealed a composition of 8.20% Cu, 5.99% Ni, 83.04% O, and 2.78% Au.*

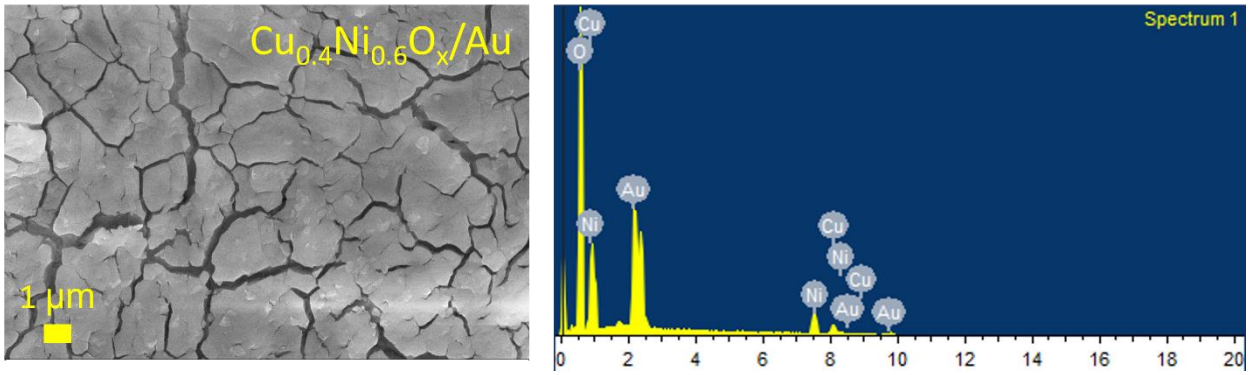

Figure S4. *SEM Image and EDX spectrum for $Cu_{0.4}Ni_{0.6}O_x$/Au as-prepared electrode. EDX revealed a composition of 6.24% Cu, 8.28% Ni, 82.00% O, and 3.47% Au.*

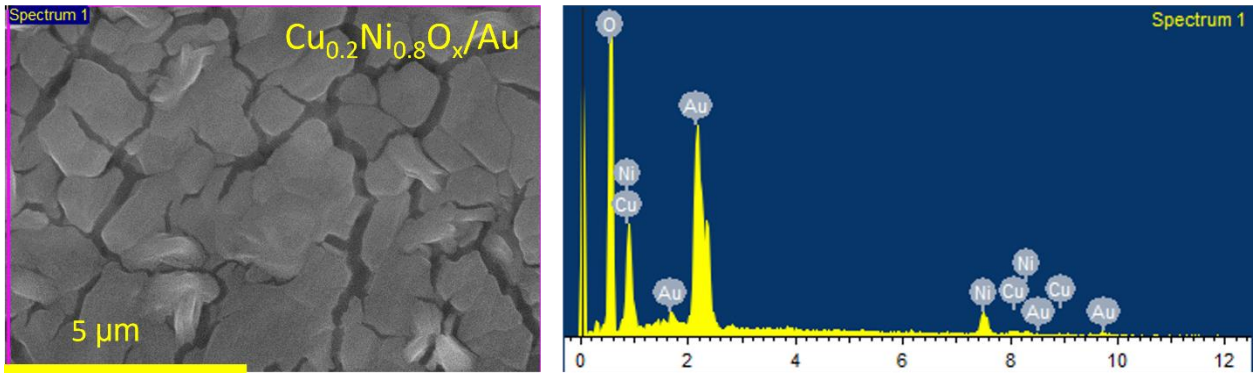

Figure S5. *SEM Image and EDX spectrum for $Cu_{0.2}Ni_{0.8}O_x$/Au as-prepared electrode. EDX revealed a composition of 2.58% Cu, 8.72% Ni, 82.61% O, and 6.09% Au.*

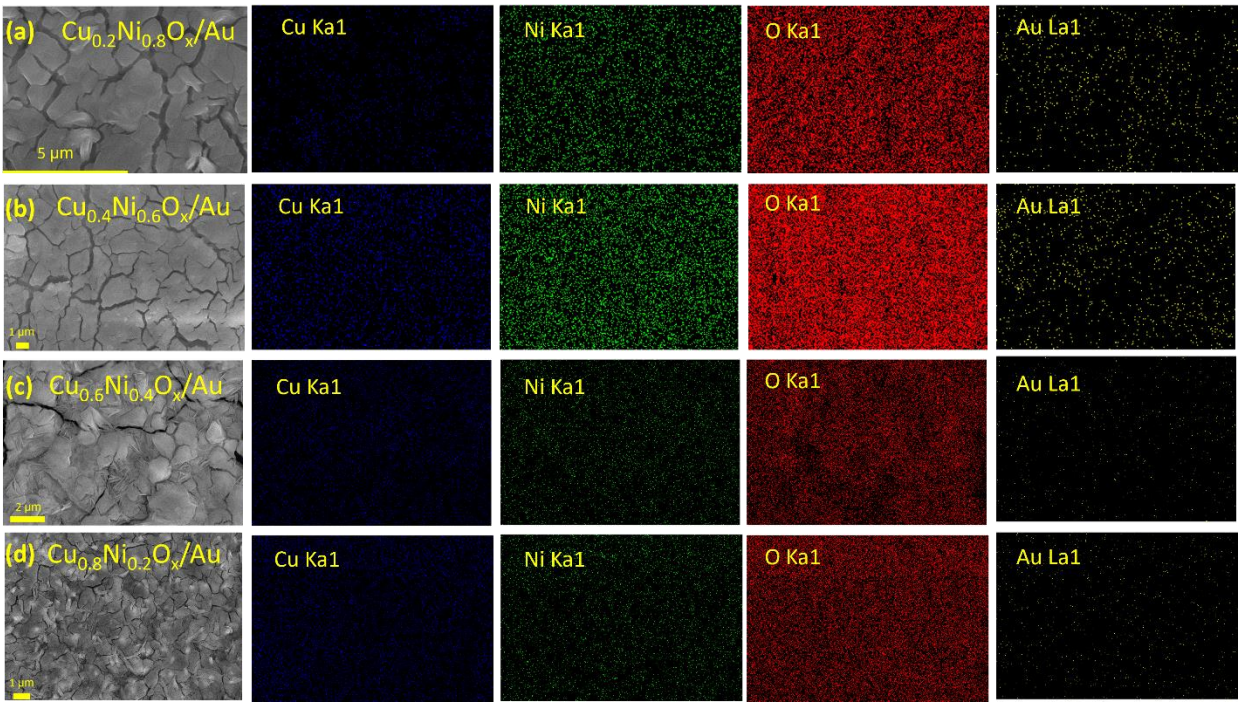

Figure S6. *SEM Image and EDX mapping of Cu, Ni, O, and Au for as-prepared (a) $Cu_{0.2}Ni_{0.8}O_x$/Au, (c) $Cu_{0.4}Ni_{0.6}O_x$/Au, (c) $Cu_{0.6}Ni_{0.4}O_x$/Au, and (d) $Cu_{0.8}Ni_{0.2}O_x$/Au electrodes.*

VI. Electrochemical measurements of $Cu_{0.8}Ni_{0.2}O_x$/Au catalyst under N_2 and O_2-saturated Electrolyte

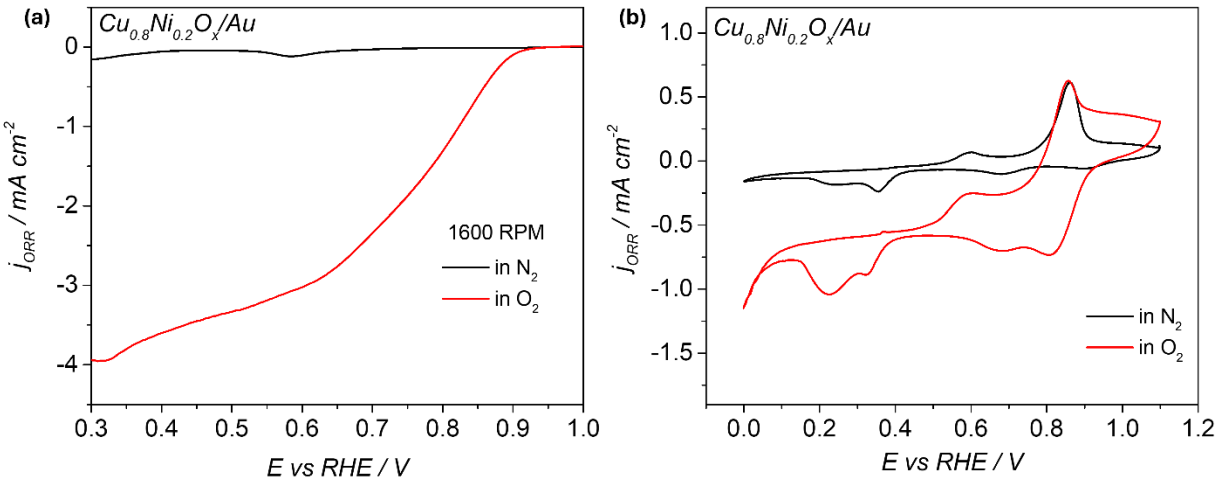

Figure S7. (*a) Linear sweep voltammograms (RDE) in N_2 and O_2-Saturated 0.1 M NaOH Electrolyte at 1600 rpm. (b) Cyclic voltammograms of $Cu_{0.8}Ni_{0.2}O_x$/Au in N_2 and O_2-saturated 0.1 M NaOH solutions.*

VII. Cyclic voltammogram of Cu[Ni]O_x/Au and CuO_x/Au in Argon

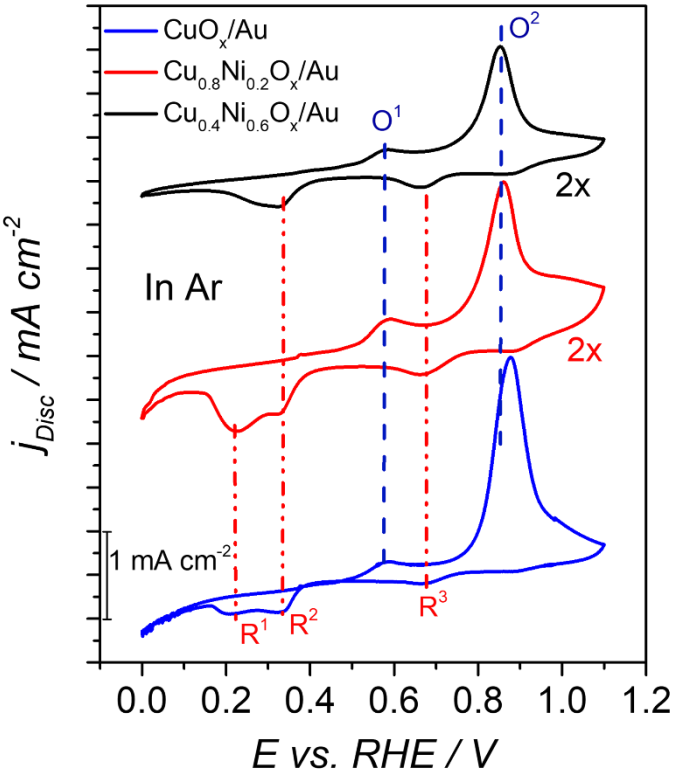

Figure S8. *Cyclic voltammograms of $Cu_{0.8}Ni_{0.2}O_x$/Au, $Cu_{0.4}Ni_{0.6}O_x$/Au, and CuO_x/Au in Ar-saturated 0.1 M NaOH solutions are shown. The oxidation and reduction peaks are denoted by the letters O^n and R^n, respectively.*

VIII. Cyclic Voltammogram (CV) of Cu[Ni]O_x Catalysts

Cyclic voltammograms (CV) of doped Cu[Ni]O_x/Au catalysts were performed to understand the redox features of Cu and Ni. We observed that Cu redox features dominated all the CVs.

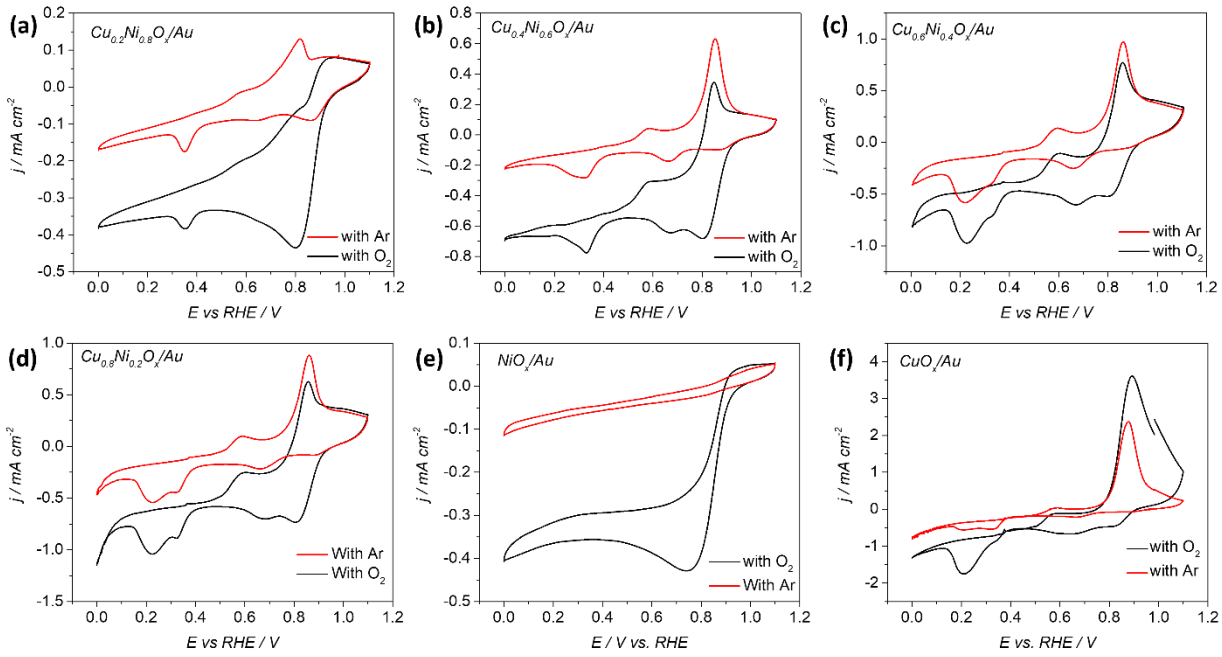

Figure S9. *Cyclic Voltammetry (CV) of as-prepared Cu[Ni]O_x/Au catalysts in O_2 (black) and Ar (red) saturated 0.1 M NaOH solution (potential scan rate: 20 mV s^{-1}). (a) $Cu_{0.2}Ni_{0.8}O_x$/Au, (b) $Cu_{0.4}Ni_{0.6}O_x$/Au, (c) $Cu_{0.6}Ni_{0.4}O_x$/Au, (d) $Cu_{0.8}Ni_{0.2}O_x$/Au, (e) NiO_x/Au, and (f) CuO_x/Au.*

IX. **Table S1:** Lists the redox peaks of Cu[Ni]O_x/Au and CuO_x/Au. **Figures 1(c) and S8** show the labels for the oxidation and reduction peaks. Referencing Caballero-Briones, F. et al. for the reference potentials.[4,5]

Peak Name	**Peak position (E/V vs. RHE)**			**Peak assigned**	**Reference potential (E/V vs. RHE)**
	$Cu_{0.8}Ni_{0.2}O_x$/Au	$Cu_{0.4}Ni_{0.6}O_x$/Au	CuO_x/Au		
O^1	0.58	0.58	0.58	$Cu^0 \rightarrow Cu^{1+}$	~ 0.59
O^2	0.85	0.58	> 0.85	Cu^0, $Cu^{1+} \rightarrow Cu^{2+}$	~ 0.85 and 1.02
R^1	0.21	-	0.21	Cu^{2+} ,$Cu^{1+} \rightarrow Cu^0$	~ 0.15
R^2	0.34	0.34	0.34	Cu^{2+} ,$Cu^{1+} \rightarrow Cu^0$	-
R^3	0.68	0.68	0.68	$Cu^{2+} \rightarrow Cu^{1+}$	~ 0.47
R^4	0.82	0.82	0.82	ORR	-

X. Supplementary note 1: Estimation of kinetic currents for Cu[Ni]O_x/Au, CuO_x/Au, and NiO_x/Au electrodes

Koutecky-Levich plots of 1/j vs. $1/\omega^{1/2}$ were used to obtain the kinetic current value (j_K) as per the equation.

$$1/j = 1/B\omega^{1/2} + 1/j_K.$$

Where j = total current density, ω = rotation rate of the electrode (in rps), and j_K = kinetic current density. The j_K values were obtained from the intercepts of the Koutecky-Levich plots.

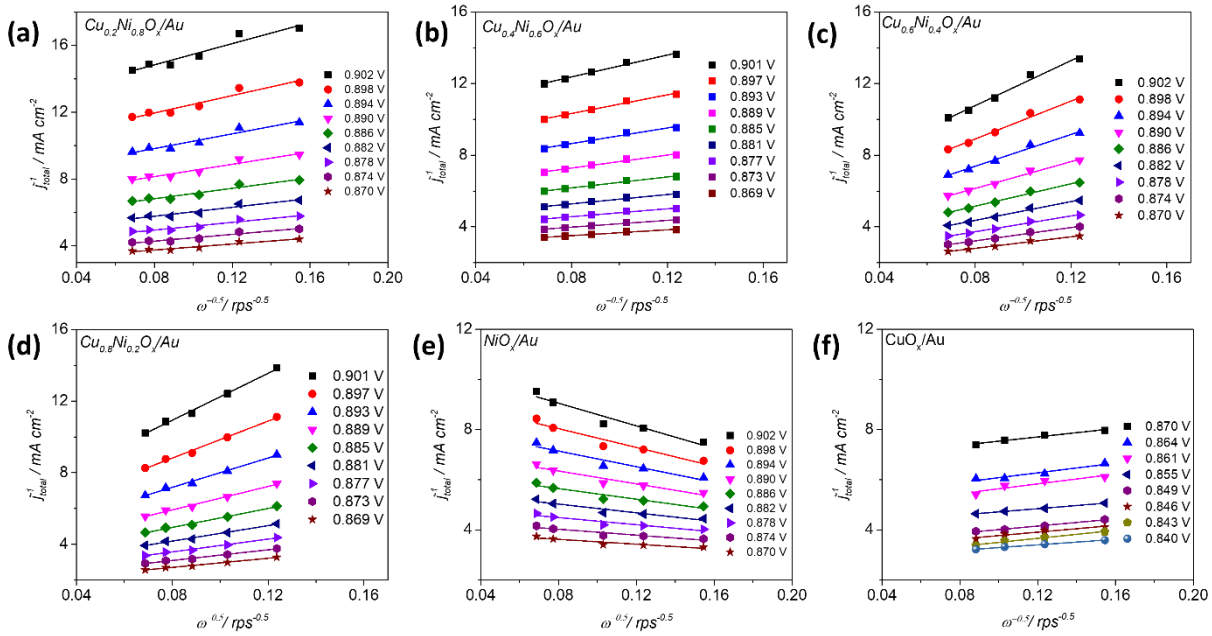

Figure S10. *Koutecky-Levich plots for various Cu[Ni]O_x/Au, CuO_x/Au, and NiO_x/Au electrodes.*

XI. Table S2: Lists Various performance parameters, such as ORR current density, electron transfer number (n), H_2O_2 yield, Tafel slope, and electrochemical surface area (ECSA) of various electrodes, are listed.

Catalysts	j_{ORR} (at 0.6 V) (mA cm^{-2})	n (at 0.6 V)	% of H_2O_2 yield	Tafel slope (mV/dec)	ECSA (cm^2)
$Cu_{0.2}Ni_{0.8}O_x$/Au	-2.45	3.82	8.79	53	0.687
$Cu_{0.4}Ni_{0.6}O_x$/Au	-2.33	3.92	3.82	59	0.621
$Cu_{0.6}Ni_{0.4}O_x$/Au	-2.67	3.913	4.31	55	0.633
$Cu_{0.8}Ni_{0.2}O_x$/Au	-3.02	3.908	4.6	60	0.776
NiO_x/Au	-1.87	3.32	34.23	74	0.291
CuO_x/Au	-2.1	3.64	18.23	73	5.189

XII. Supplementary note 2: Calculation of ECSA of various catalysts

The electrochemically active surface area (ECSA) of various electrocatalysts, such as Cu[Ni]O_x/Au, pure CuO_x/Au, and NiO_x/Au, were estimated using electrochemical double-layer capacitance. The double-layer capacitance was calculated from the non-faradaic region of cyclic voltammograms obtained at varying scan rates. A specific capacitance (C_s) value of 40 μF cm^{-2} for a flat surface was used for ECSA calculations. Currents were plotted against scan rates. The Double-layer capacitance (C_{DL}) was estimated by averaging the slopes of current vs. scan rate plots.[6] The ECSA was obtained by normalizing the double-layer capacitance by a specific capacitance value: ECSA= C_{DL}/C_s.

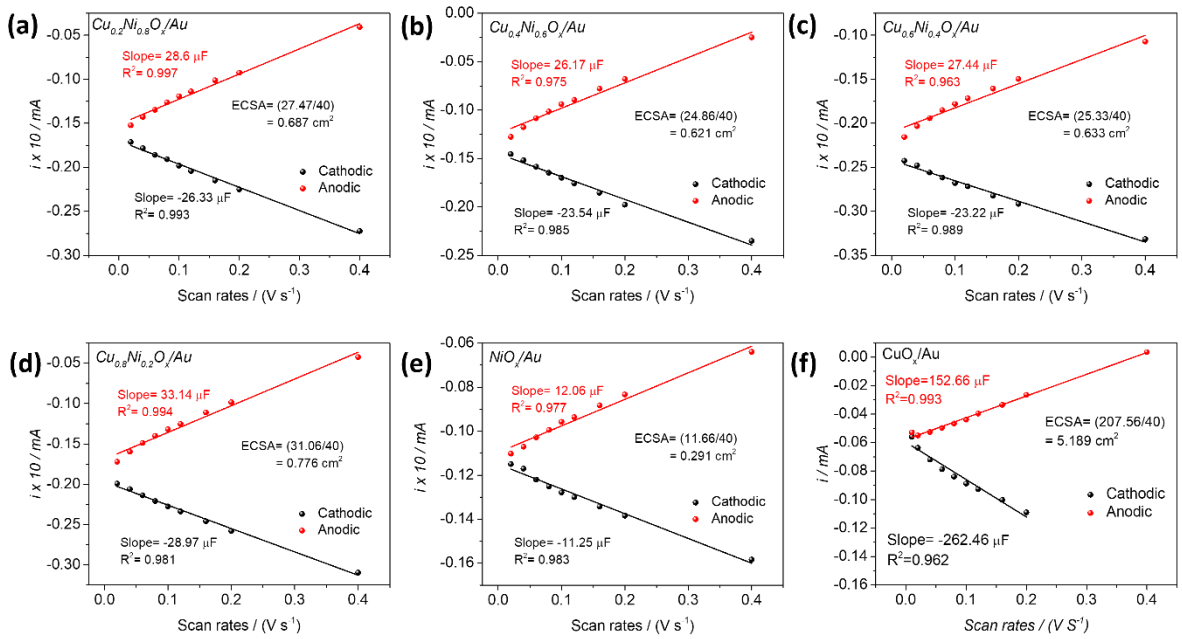

Figure S11. *Plots of charging current (anodic and cathodic) vs. scan rates are shown. Where (a) $Cu_{0.2}Ni_{0.8}O_x$/Au, (b) $Cu_{0.4}Ni_{0.6}O_x$/Au, (c) $Cu_{0.6}Ni_{0.4}O_x$/Au, (d) $Cu_{0.8}Ni_{0.2}O_x$/Au, (e) NiO_x/Au, and (f) CuO_x/Au.*

XIII. Impedance spectra of Cu[Ni]O_x/Au electrodes at 0.6 V

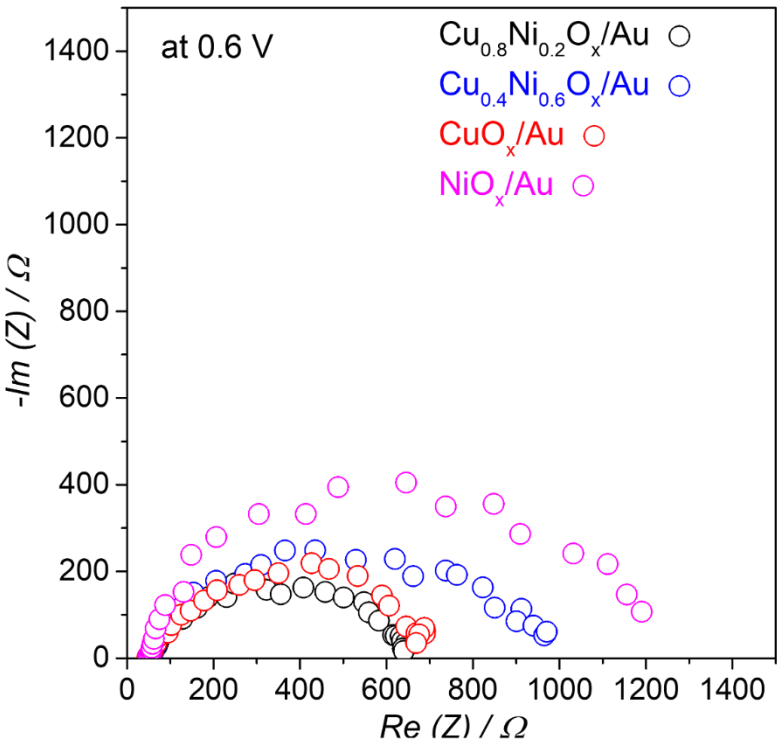

Figure S12. *Electrochemical impedance spectroscopy (EIS) plots are obtained at an operating potential of 0.6 V in O_2-saturated 0.1M NaOH. An electrode rotation rate of 1600 rpm was used.*

XIV. Performance stability of Cu[Ni]O_x/Au electrodes

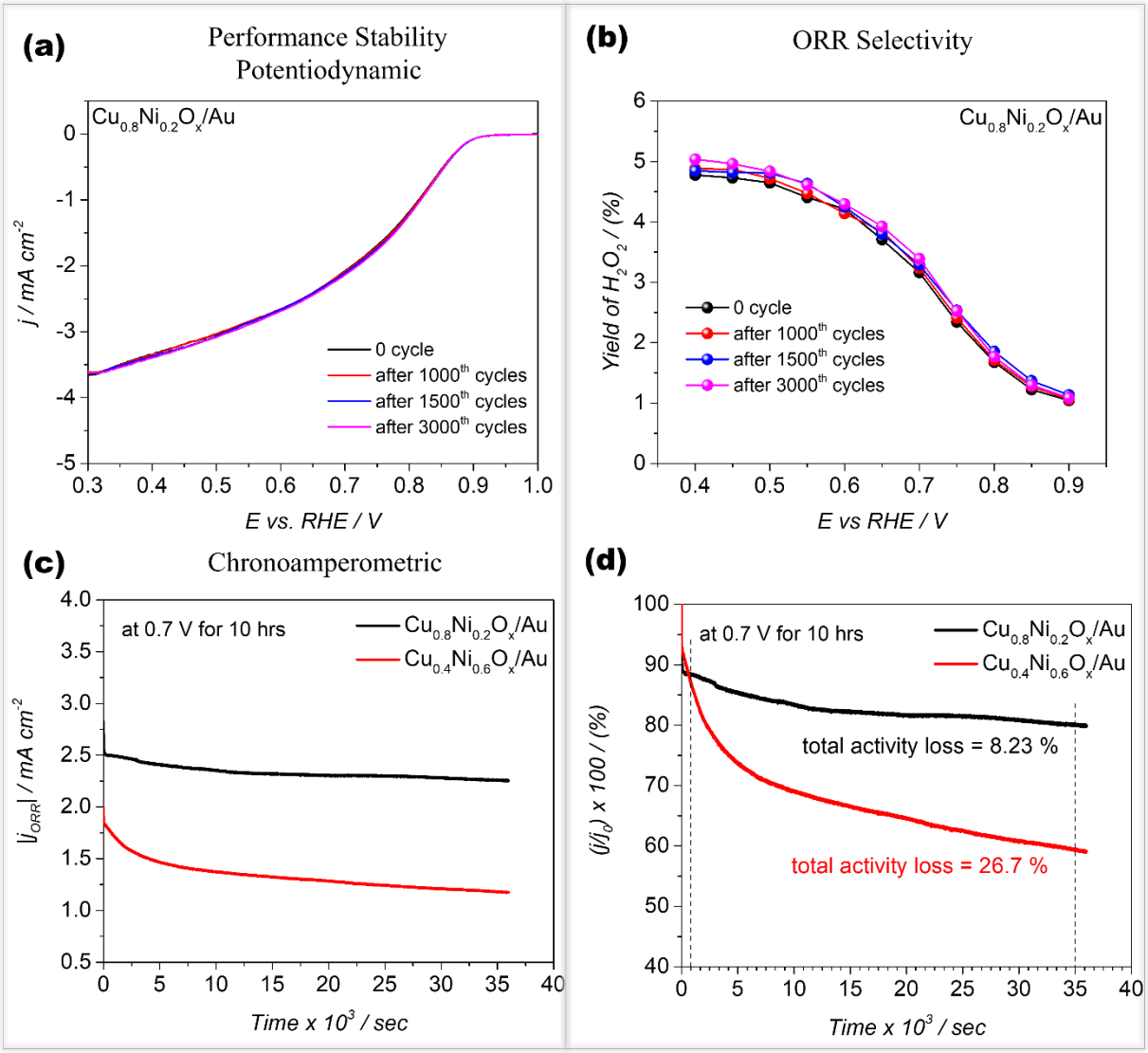

Figure S13. *(a) $Cu_{0.8}Ni_{0.2}O_x$/Au polarization curves were measured in 0.1 M NaOH under O_2-saturation. Experimental conditions included a 5 mVs^{-1} scan rate and 1600 rpm electrode rotation speed. Potential cycling of the electrode occurred at a rate of 100 mVs^{-1} from 0.6 to 1.0 V. The polarization curves obtained after completing the 1000th, 1500th, and 3000th potential cycles are compared with the initial polarization curve. (b) The yield of H_2O_2 (%) before and after the 1000th, 1500th, and 3000th cycles. (c) The chronoamperometric performance of*

$Cu[Ni]O_x$/Au ($Cu_{0.8}Ni_{0.2}O_x$/Au and $Cu_{0.4}Ni_{0.6}O_x$/Au) at 0.7 V in O_2-saturated 0.1 M NaOH. A rotational speed of 1600 RPM was applied to the electrode. The value of $|j_{ORR}|$ was plotted against time. (d) Stability performance of $Cu[Ni]O_x$/Au ($Cu_{0.8}Ni_{0.2}O_x$/Au and $Cu_{0.4}Ni_{0.6}O_x$/Au) electrodes under constant potential (0.7 V vs RHE) for 10 hours in O_2-saturated 0.1M NaOH at 1600 RPM {normalized current (to value at time~0) vs. duration of experiment}.

XV. In-situ Raman spectra of CuO_x/Au

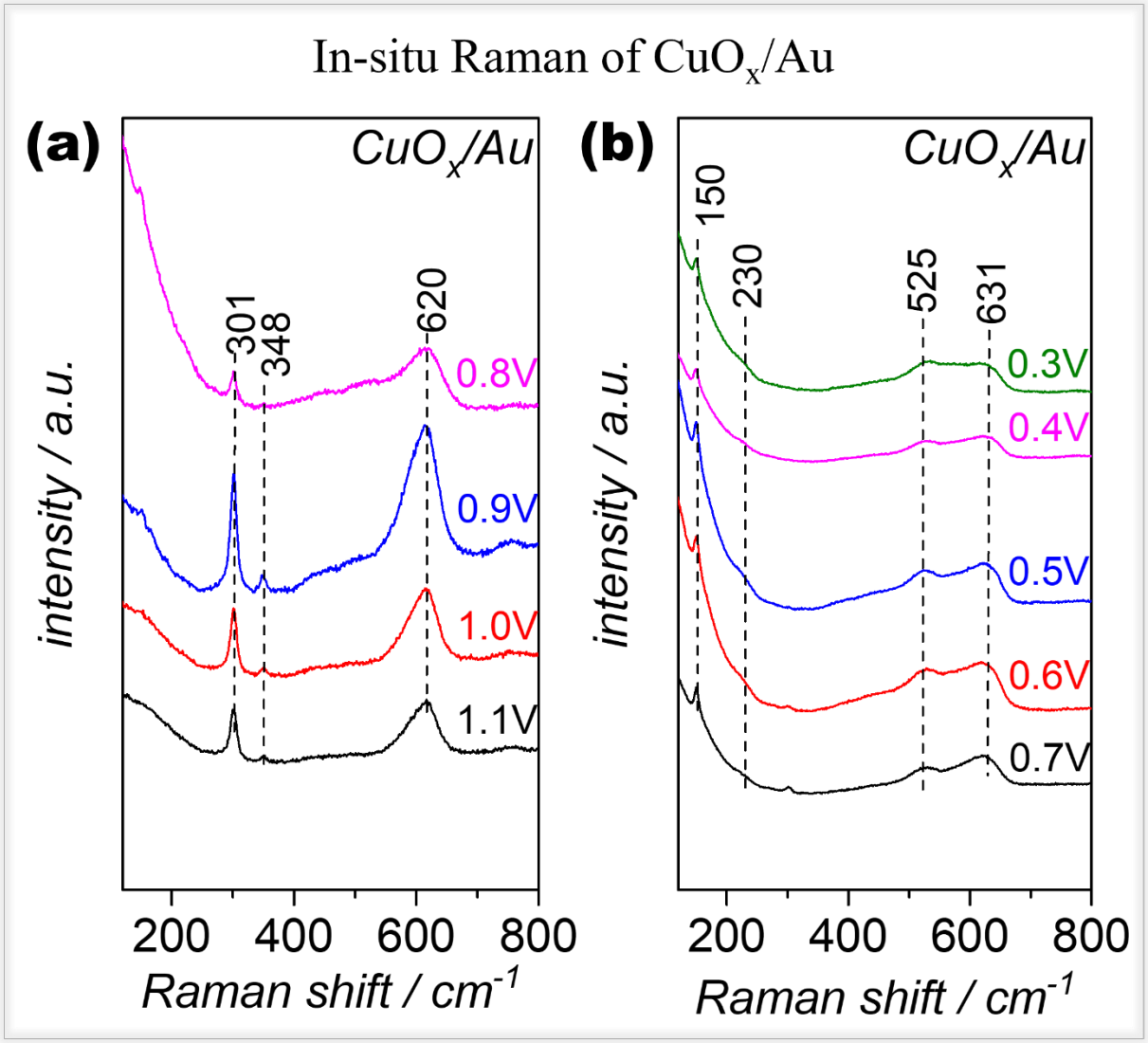

Figure S14. *In-situ Raman spectra of CuO_x/Au catalyst in O_2-saturated 0.1 M NaOH obtained under steady state conditions. The potential was varied stepwise from 1.1 V to 0.3 V.*

XVI. **Table S3**. Raman bands of various Ni and Cu oxides and hydroxides.

Phases	**Raman bands (cm^{-1})**	**References**
Cu_2O	150, 528, 623	7
	150, 220, 415, 520, 630	8
	150, 230, 525, 631	1
CuO	301, 348, 620	1
	303, 350, 636	9
	298, 347, 591	10
α-$Ni(OH)_2$	317, 451, 710, 988, 1045, 3581, 3668	11
	306, 460, 524, 3656	12
β- $Ni(OH)_2$	318, 449, 3580	11
	306, 445, 510, 3579	12
	313, 448, 3580	13
		14
	313, 453, 3583	
NiO	196, 397, 511, 551, 785, 943, 1098, 1430	15
	400, 455, 505, 540, 600	16
	400, 580, 730, 906, 1090	17
	415-421, 455-459, 500, 525-541, 580-587	18
	460, 500	19

XVII. In-situ Raman spectra of $Cu_{0.4}Ni_{0.6}O_x$/Au

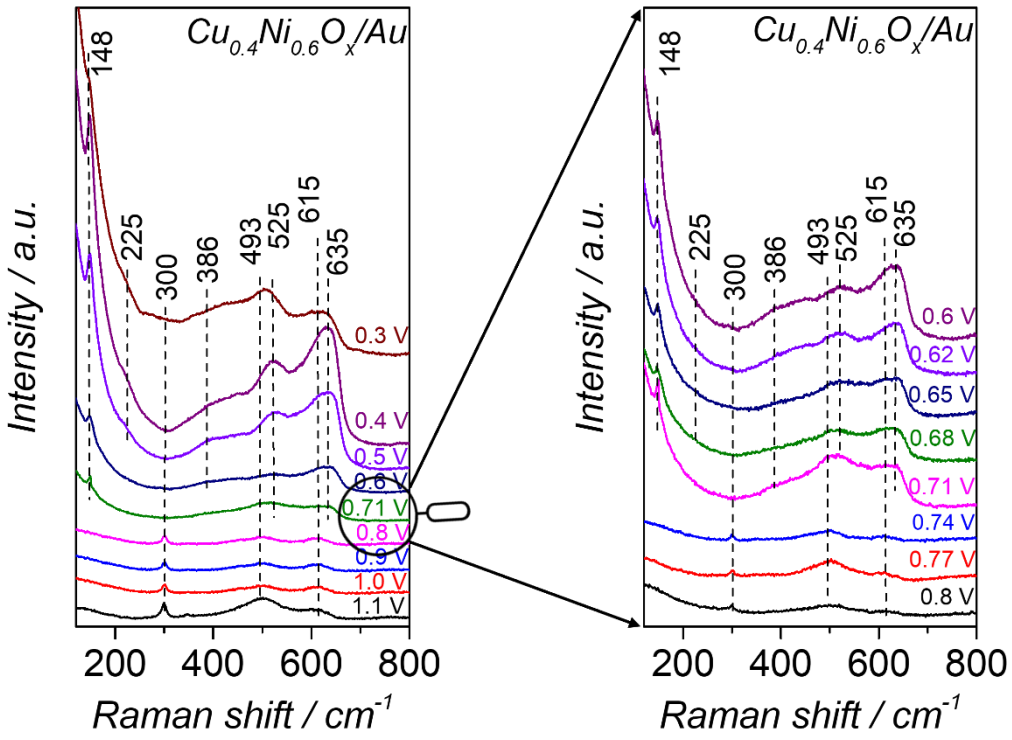

Figure S15. *In-situ Raman spectra of $Cu_{0.4}Ni_{0.6}O_x$/Au catalyst in O_2-saturated 0.1 M NaOH obtained under steady-state conditions. The potential was varied stepwise from 1.1 V to 0.3 V. The spectra are similar to spectra reported for $Cu_{0.8}Ni_{0.2}O_x$/Au in the main text.*

XVIII. In-situ Raman spectra of $Cu_{0.8}Ni_{0.2}O_x$/Au and NiO_x/Au in D_2O and H_2O_2 (0.6 V)

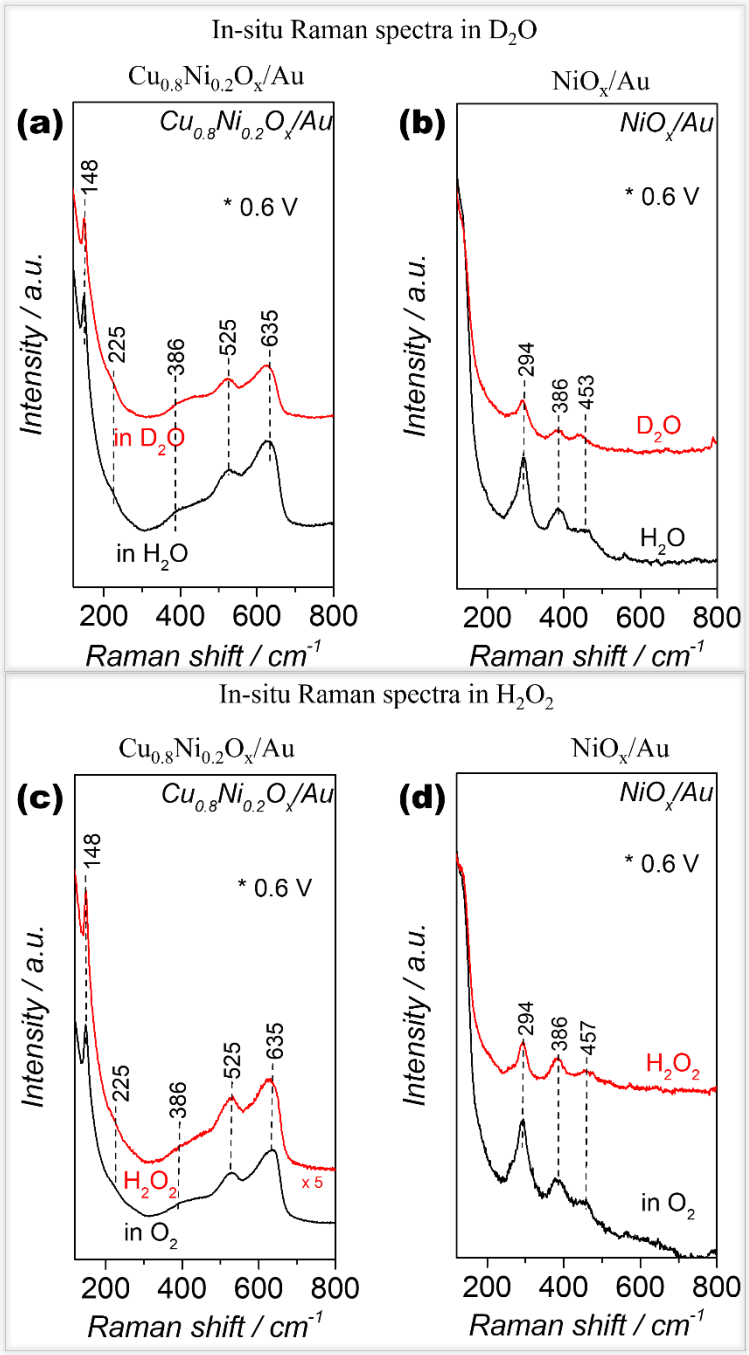

Figure S16. *In-situ Raman spectroscopy measurements were conducted at a potential of 0.6 V using $Cu_{0.8}Ni_{0.2}O_x$/Au electrodes in both D_2O (a) and H_2O_2 in H_2O (c). Using NiO_x/Au electrodes in D_2O (b) and H_2O_2 in H_2O (d). O_2-saturated 0.1 M NaOH was used as electrolyte for all experiments.*

XIX. In-situ Raman spectra of $Cu_{0.8}Ni_{0.2}O_x$/Au in D_2O (1.1 V-0.3 V)

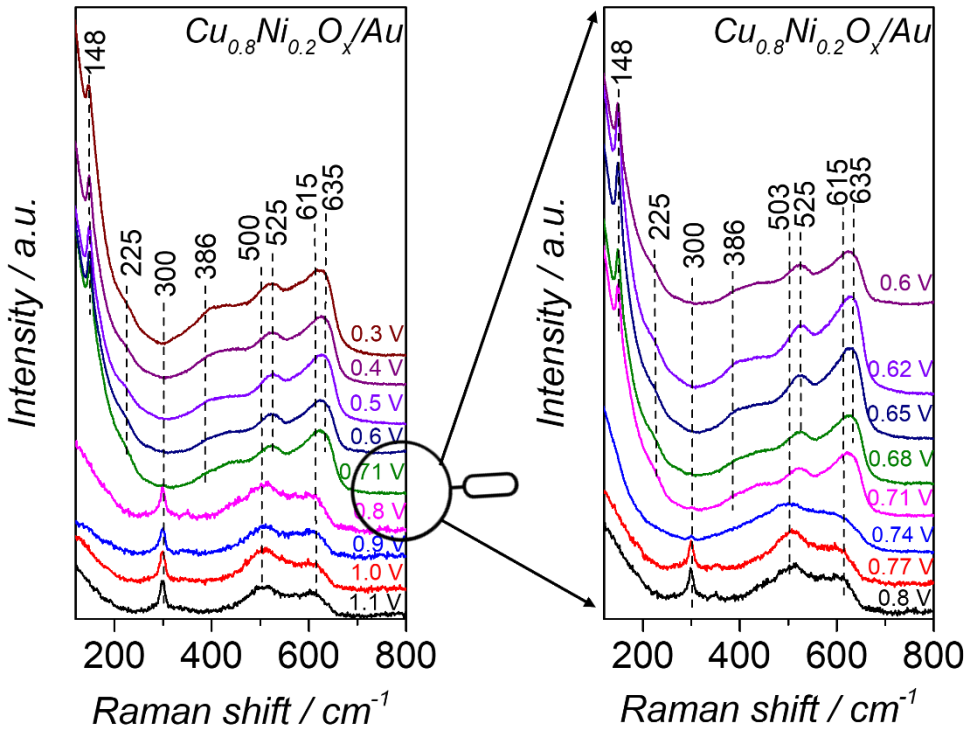

Figure S17. *In-situ Raman spectra of $Cu_{0.8}Ni_{0.2}O_x$/Au catalyst in O_2-saturated 0.1 M NaOH in D_2O obtained under steady-state conditions. The potential is varied from 1.1 V to 0.3 V.*

XX. In-situ Raman spectra NiO_x/Au in D_2O (1.1 V-0.3 V)

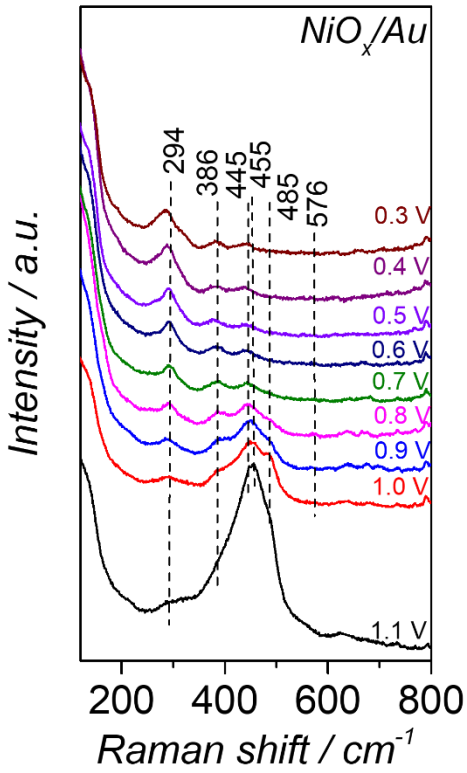

Figure S18. *In-situ Raman spectra of NiO_x/Au catalysts in O_2-saturated 0.1 M NaOH in D_2O obtained under steady-state conditions. The potential is varied from 1.1 V to 0.3 V.*

References:

(1) Biswal, S. K.; Ranjan, C. Suppressing H2O2 Formation in the Oxygen Reduction Reaction Using Co-Doped Copper Oxide Electrodes. *J. Mater. Chem. A* **2022**, *10* (41), 22042–22057. https://doi.org/10.1039/D2TA04349A.

(2) Das, A.; Mohapatra, B.; Kamboj, V.; Ranjan, C. Promotion of Electrochemical Water Oxidation Activity of Au Supported Cobalt Oxide upon Addition of Cr: Insights Using in Situ Raman Spectroscopy. *ChemCatChem* **2021**, *13* (8), 2053–2063. https://doi.org/10.1002/cctc.202001889.

(3) Liu, Y.-C.; Wang, C.-C.; Tsai, C.-E. Effects of Electrolytes Used in Roughening Gold Substrates by Oxidation–Reduction Cycles on Surface-Enhanced Raman Scattering. *Electrochem. Commun.* **2005**, *7* (12), 1345–1350. https://doi.org/10.1016/j.elecom.2005.09.030.

(4) Caballero-Briones, F.; Artés, J. M.; Díez-Pérez, I.; Gorostiza, P.; Sanz, F. Direct Observation of the Valence Band Edge by in Situ ECSTM-ECTS in p-Type Cu_2O Layers Prepared by Copper Anodization. *J. Phys. Chem. C* **2009**, *113* (3), 1028–1036. https://doi.org/10.1021/jp805915a.

(5) Abd el Haleem, S. M.; Ateya, B. G. Cyclic Voltammetry of Copper in Sodium Hydroxide Solutions. *J. Electroanal. Chem. Interfacial Electrochem.* **1981**, *117* (2), 309–319. https://doi.org/10.1016/S0022-0728(81)80091-5.

(6) McCrory, C. C. L.; Jung, S.; Peters, J. C.; Jaramillo, T. F. Benchmarking Heterogeneous Electrocatalysts for the Oxygen Evolution Reaction. *J. Am. Chem. Soc.* **2013**, *135* (45), 16977–16987. https://doi.org/10.1021/ja407115p.

(7) Niaura, G. Surface-Enhanced Raman Spectroscopic Observation of Two Kinds of Adsorbed OH^- Ions at Copper Electrode. *Electrochim. Acta* **2000**, *45* (21), 3507–3519. https://doi.org/10.1016/S0013-4686(00)00434-5.

(8) Singhal, A.; Pai, M. R.; Rao, R.; Pillai, K. T.; Lieberwirth, I.; Tyagi, A. K. Copper(I) Oxide Nanocrystals – One Step Synthesis, Characterization, Formation Mechanism, and Photocatalytic Properties. *Eur. J. Inorg. Chem.* **2013**, *2013* (14), 2640–2651. https://doi.org/10.1002/ejic.201201382.

(9) Chen, X. K.; Irwin, J. C.; Franck, J. P. Evidence for a Strong Spin-Phonon Interaction in Cupric Oxide. *Phys. Rev. B* **1995**, *52* (18), R13130–R13133. https://doi.org/10.1103/PhysRevB.52.R13130.

(10) Deng, Y.; Handoko, A. D.; Du, Y.; Xi, S.; Yeo, B. S. In Situ Raman Spectroscopy of Copper and Copper Oxide Surfaces during Electrochemical Oxygen Evolution Reaction: Identification of CuIII Oxides as Catalytically Active Species. *ACS Catal.* **2016**, *6* (4), 2473–2481. https://doi.org/10.1021/acscatal.6b00205.

(11) Johnston, C.; Graves, P. R. *In Situ* Raman Spectroscopy Study of the Nickel Oxyhydroxide Electrode (NOE) System. *Appl Spectrosc* **1990**, *44* (1), 105–115. https://doi.org/10.1366/0003702904085769.

(12) Kostecki, R.; McLarnon, F. Electrochemical and In Situ Raman Spectroscopic Characterization of Nickel Hydroxide Electrodes: I. Pure Nickel Hydroxide. *J. Electrochem. Soc.* **1997**, *144* (2), 485–493. https://doi.org/10.1149/1.1837437.

(13) Yu, X.; Zhao, J.; Zheng, L.-R.; Tong, Y.; Zhang, M.; Xu, G.; Li, C.; Ma, J.; Shi, G. Hydrogen Evolution Reaction in Alkaline Media: Alpha- or Beta-Nickel Hydroxide on the Surface of Platinum? *ACS Energy Lett.* **2018**, *3* (1), 237–244. https://doi.org/10.1021/acsenergylett.7b01103.

(14) Bernard, M. C.; Keddam, M.; Takenouti, H.; Bernard, P.; Sényarich, S. Electrochemical Behavior of Quasi-Spherical β - Ni (OH) 2 Particles Studied by Roman Spectroscopy. *J. Electrochem. Soc.* **1996**, *143* (8), 2447–2451. https://doi.org/10.1149/1.1837029.
(15) Şenaslan, F.; Taşdemir, M.; Çelik, A. Effect of Working Pressure and Post-Annealing on Structural, Optical and Electrical Properties of p-Type NiO Thin Films Produced by RF Magnetron Sputtering Technique. *Appl. Phys. A* **2021**, *127* (10), 739. https://doi.org/10.1007/s00339-021-04901-2.
(16) Qiu, J.; Nguyen, T. H.; Kim, S.; Lee, Y. J.; Song, M.-T.; Huang, W.-J.; Chen, X.-B.; Nguyen, T. M. H.; Yang, I.-S. Two-Dimensional Correlation Spectroscopy Analysis of Raman Spectra of NiO Nanoparticles. *Spectrochim. Acta, Part A* **2022**, *280*, 121498. https://doi.org/10.1016/j.saa.2022.121498.
(17) Mironova-Ulmane, N.; Kuzmin, A.; Sildos, I.; Puust, L.; Grabis, J. Magnon and Phonon Excitations in Nanosized NiO. *Latvian J. Phys. Tech. Sci.* **2019**, *56* (2), 61–72. https://doi.org/10.2478/lpts-2019-0014.
(18) Bala, N.; Singh, H. K.; Verma, S.; Rath, S. Magnetic-Order Induced Effects in Nanocrystalline NiO Probed by Raman Spectroscopy. *Phys. Rev. B* **2020**, *102* (2), 024423. https://doi.org/10.1103/PhysRevB.102.024423.
(19) Chan, S. S.; Wachs, I. E. In-Situ Laser Raman Spectroscopy of Nickel Oxide Supported on. Gamma. -Al/Sub 2/O/Sub 3/. *J. Catal.; (United States)* **1987**, *103:1*.